

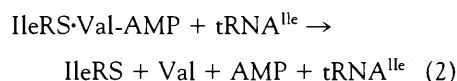
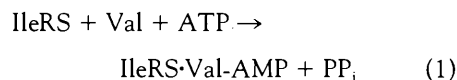
# Enzyme Structure with Two Catalytic Sites for Double-Sieve Selection of Substrate

Osamu Nureki, Dmitry G. Vassilyev, Masaru Tateno, Atsushi Shimada, Takashi Nakama, Shuya Fukai, Mitiko Konno, Tamara L. Hendrickson, Paul Schimmel, Shigeyuki Yokoyama\*

High-fidelity transfers of genetic information in the central dogma can be achieved by a reaction called editing. The crystal structure of an enzyme with editing activity in translation is presented here at 2.5 angstroms resolution. The enzyme, isoleucyl-transfer RNA synthetase, activates not only the cognate substrate L-isoleucine but also the minimally distinct L-valine in the first, aminoacylation step. Then, in a second, "editing" step, the synthetase itself rapidly hydrolyzes only the valylated products. For this two-step substrate selection, a "double-sieve" mechanism has already been proposed. The present crystal structures of the synthetase in complexes with L-isoleucine and L-valine demonstrate that the first sieve is on the aminoacylation domain containing the Rossmann fold, whereas the second, editing sieve exists on a globular  $\beta$ -barrel domain that protrudes from the aminoacylation domain.

Editing reactions are essential for the high fidelity of genetic information transfer in replication and translation (error rates of 1/2400 to 1/40,000) (1, 2). Translation accuracy depends on the editing activities of aminoacyl-tRNA synthetases (aaRSs) (2–4). The aaRSs esterify cognate amino acids with their specific tRNAs, which decode trinucleotide sequences (anticodons) into amino acids corresponding strictly to the genetic code. The amino acid and adenosine triphosphate (ATP) form an aminoacyl adenylate as an active intermediate, and the aminoacyl moiety is then transferred to the 3' terminal adenosine of the tRNA. The accuracy of protein biosynthesis depends on the correct recognition of amino acids and tRNAs by aaRSs. Discrimination between L-isoleucine and L-valine is one of the most difficult recognitions to achieve, because they differ by only one methylene group in their aliphatic side chains. Pauling estimated, from a value of about 1 kcal mol<sup>-1</sup> for the hydrophobic binding energy

of a methylene group, the error rate for L-valine replacing L-isoleucine to be about one in five (5). Thus, it is thermodynamically impossible for isoleucyl-tRNA synthetase (IleRS) to achieve strict discrimination [an error rate as low as 1/40,000 (3)] between L-isoleucine and L-valine through ordinary one-step recognition. Actually, IleRS has an additional editing activity that hydrolyzes both valyl-adenosine monophosphate (Val-AMP) and Val-tRNA<sup>Ile</sup> in a tRNA<sup>Ile</sup>-dependent manner (2–4, 6, 7), as follows:



where PP<sub>i</sub> is inorganic pyrophosphate. In Eq. 1, the L-valine is activated. In Eq. 2, tRNA-dependent editing occurs. In this overall reaction, the Val-AMP is directly hydrolyzed to Val + AMP in a pretransfer editing, and, in addition, some Val-tRNA<sup>Ile</sup> forms, which is deacylated by the enzyme (posttransfer editing). The overall editing reaction (including both) is measured by the hydrolysis of ATP in the presence of L-valine and tRNA<sup>Ile</sup>. Fersht first proposed a "double-sieve" model for two-step substrate selection (2): Amino acids larger than the cognate L-isoleucine are strictly excluded by the first, amino acid activation site, serving as the "coarse sieve," and smaller ones, such as L-valine, are strictly eliminated by the "fine sieve" of the second hydrolytic site. The site for editing is distinct from that for amino acid activation (6, 8, 9). In addition to IleRS, valyl-tRNA synthetase (ValRS) has similar editing ac-

tivities against an isosteric substrate, L-threonine (3, 7).

The crystal structure of *Thermus thermophilus* IleRS (1045 amino acid residues, 120 kD) and those of the complexes of IleRS with L-isoleucine and L-valine were determined at resolutions of 2.5, 2.8, and 2.8 Å, respectively (Table 1) (10). IleRS belongs to the class I synthetases (11), which are characterized by an ATP-binding domain constructed with a Rossmann fold. *Thermus thermophilus* IleRS is a thick, L-shaped molecule with an approximate size of 100 Å by 80 Å by 45 Å (Fig. 1). The IleRS structure exhibits the Rossmann-fold domain at the center,  $\beta$ -rich intervening domains at the top, and an  $\alpha$ -rich cylindrical domain at the bottom (Fig. 1).

The Rossmann-fold domain (shown in orange in Fig. 1) has a central deep catalytic cleft with two characteristic ATP-binding motifs, His<sup>54</sup>-Val<sup>55</sup>-Gly<sup>56</sup>-His<sup>57</sup> and Lys<sup>591</sup>-Met<sup>592</sup>-Ser<sup>593</sup>-Lys<sup>594</sup>, on its lower level. In the L-isoleucine-IleRS complex, one L-isoleucine molecule is bound at the bottom of this catalytic cleft (Fig. 2, A and B). The hydrophobic side chain of L-isoleucine is

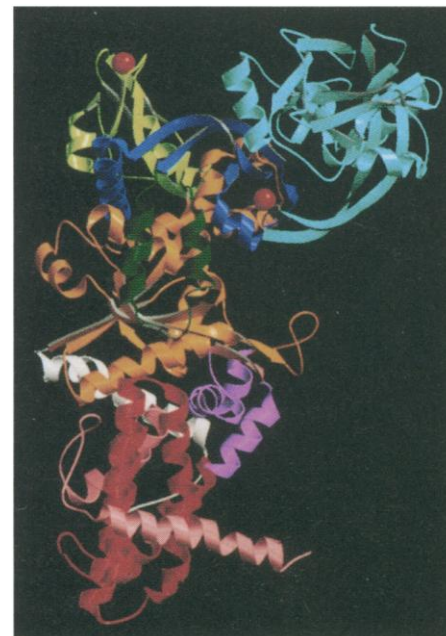


**Fig. 1.** Schematic drawing of the structure of *T. thermophilus* IleRS. The NH<sub>2</sub>-terminal extension, the Rossmann-fold domain, an  $\alpha$ - $\alpha$ - $\beta$ - $\alpha$  domain specific to monomeric class I synthetases (37), and the  $\alpha$ -helix bundle domain are shown in white, orange, violet, and red, respectively. The COOH-terminal 217 residues of the IleRS are partially disordered, and only two helices (shown in pink) could be traced. In addition, the IleRS has an insert, in the Rossmann-fold domain, consisting of four structural domains (Ins-1, Ins-2, Ins-3, and Ins-4 domains, as shown in blue, aqua, green, and light green, respectively). The bound Zn<sup>2+</sup> ions are represented by red balls.

O. Nureki, M. Tateno, S. Yokoyama, Department of Biophysics and Biochemistry, Graduate School of Science, University of Tokyo, 7-3-1 Hongo, Bunkyo-ku, Tokyo 113, Japan, and Institute of Physical and Chemical Research (RIKEN), 2-1 Hirosawa, Wako, Saitama 351-01, Japan.

D. G. Vassilyev, International Institute for Advanced Research, Central Research Laboratories, Matsushita Electric Industrial, 3-4 Hikari-dai, Seika, Kyoto 619-02, Japan.

A. Shimada, T. Nakama, S. Fukai, Department of Biophysics and Biochemistry, Graduate School of Science, University of Tokyo, 7-3-1 Hongo, Bunkyo-ku, Tokyo 113, Japan.

M. Konno, Department of Chemistry, Faculty of Science, Ochanomizu University, 2-1-1 Otsuka, Bunkyo-ku, Tokyo 112, Japan.

T. L. Hendrickson and P. Schimmel, Skaggs Institute for Chemical Biology, Scripps Research Institute, 10550 North Torrey Pines Road, La Jolla, CA 92037.

\*To whom correspondence should be addressed. E-mail: yokoyama@y-sun.biochem.s.u-tokyo.ac.jp

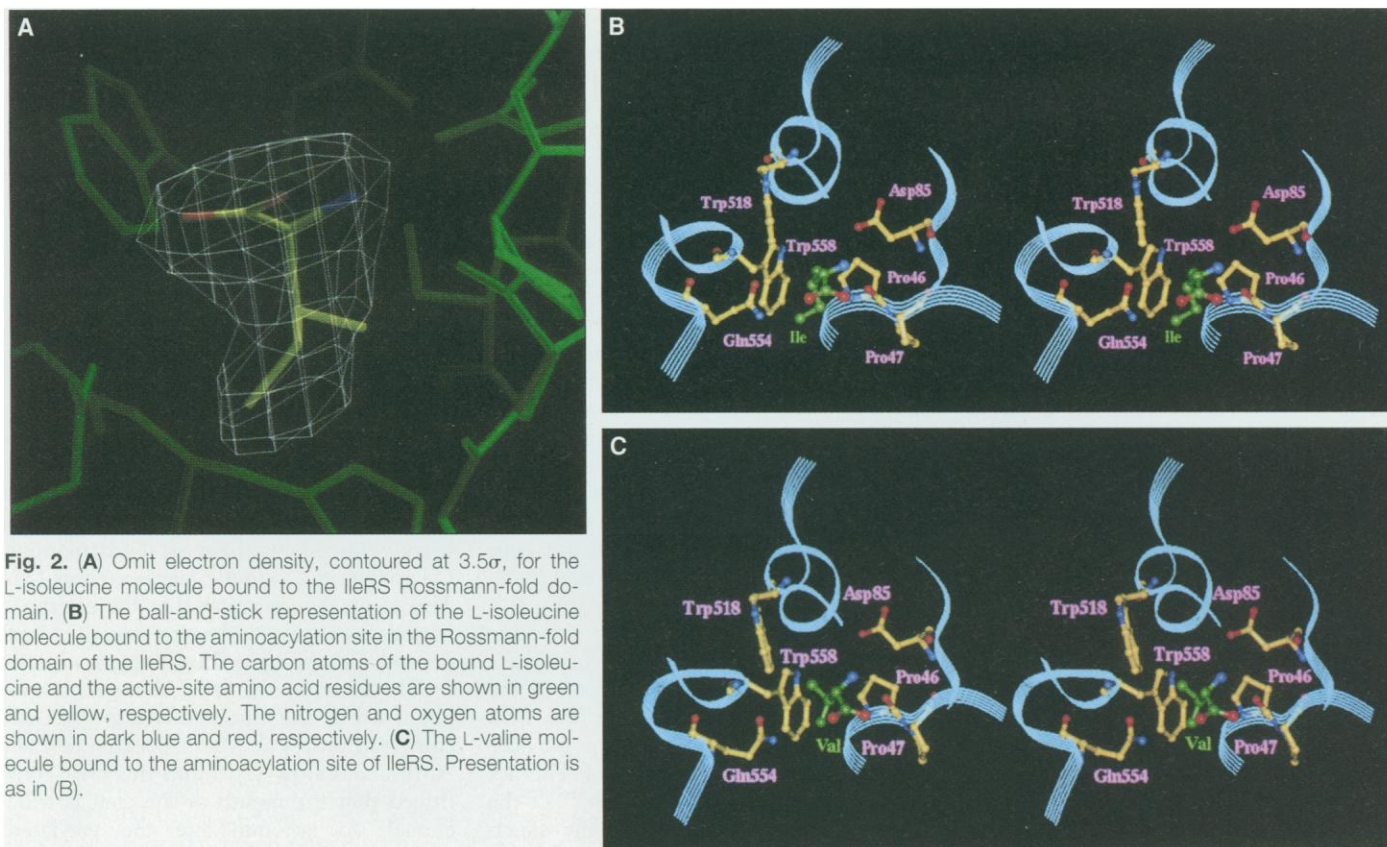


**Fig. 2.** (A) Omit electron density, contoured at  $3.5\sigma$ , for the L-isoleucine molecule bound to the IleRS Rossmann-fold domain. (B) The ball-and-stick representation of the L-isoleucine molecule bound to the aminoacylation site in the Rossmann-fold domain of the IleRS. The carbon atoms of the bound L-isoleucine and the active-site amino acid residues are shown in green and yellow, respectively. The nitrogen and oxygen atoms are shown in dark blue and red, respectively. (C) The L-valine molecule bound to the aminoacylation site of IleRS. Presentation is as in (B).

recognized by a pocket consisting of Pro<sup>46</sup>, Trp<sup>518</sup>, and Trp<sup>558</sup> through van der Waals interactions (Fig. 2B). The Asp<sup>85</sup> and Gln<sup>554</sup> residues form hydrogen bonds with

the NH<sub>3</sub><sup>+</sup> and COO<sup>-</sup> groups, respectively (Fig. 2B). These residues are completely conserved among the 17 IleRSs cloned thus far (12). The L-leucine side chain does not

fit into this pocket, because of the steric hindrance of one of the terminal methyl groups (13). Naturally, larger amino acids are occluded from this pocket. In contrast,

**Table 1.** Crystallographic data and refinement statistics (10). The crystals belong to the space group C2, with  $a = 160 \text{ \AA}$ ,  $b = 94.5 \text{ \AA}$ ,  $c = 127 \text{ \AA}$ , and  $\beta = 126^\circ$ , and contain one molecule per asymmetric unit, resulting in a solvent content of 63%. The average refined  $B$  factor of the present model is  $25.53 \text{ \AA}^2$ .

|   | Native       | IleRS + L-isoleucine | IleRS + L-valine | K3C + Hg | A132C + Hg | SEM    |
|---|--------------|----------------------|------------------|----------|------------|--------|
| <i>Diffraction data</i>                 |              |                      |                  |          |            |        |
| Resolution (Å)                          | 2.5          | 2.8                  | 2.8              | 2.8      | 2.8        | 3.0    |
| Unique reflections                      | 47,068       | 34,977               | 31,936           | 30,083   | 29,360     | 27,791 |
| Total reflections                       | 134,577†     | 116,528†             | 66,364           | 93,579   | 88,169     | 59,728 |
| $R_{\text{merge}}$ (%)*                 | 6.4 (35.2)†  | 5.1 (38.1)†          | 5.7 (40.1)†      | 6.9      | 6.5        | 4.9    |
| Completeness (%)                        | 88.5 (65.7)† | 95.3 (91.3)†         | 87.5 (86.4)†     | 97.9     | 95.8       | 90.1   |
| <i>Phasing statistics (3.0 to 50 Å)</i> |              |                      |                  |          |            |        |
| $R_{\text{der}}$ (%)‡                   |              |                      |                  | 14.0     | 17.0       | 11.0   |
| Overall phasing power§                  |              |                      |                  | 2.29     | 1.60       | 1.32   |
| $R_{\text{cullis}}$                     |              |                      |                  | 0.66     | 0.75       | 0.84   |
| <i>Refinement statistics</i>            |              |                      |                  |          |            |        |
| Resolution (Å)                          | 2.5–15       | 2.8–15               | 2.8–15           |          |            |        |
| Number of reflections                   | 46,804       | 34,034               | 30,303           |          |            |        |
| Number of protein atoms                 | 6,698        | 6,688                | 6,695            |          |            |        |
| Number of zinc ions                     | 2            | 2                    | 2                |          |            |        |
| Number of water molecules               | 322          | 0                    | 0                |          |            |        |
| rmsd bond lengths (Å)                   | 0.017        | 0.021                | 0.019            |          |            |        |
| rmsd bond angles (°)                    | 2.25         | 2.96                 | 2.92             |          |            |        |
| rmsd impropers (°)                      | 1.65         | 1.06                 | 1.03             |          |            |        |
| $R_{\text{work}}/R_{\text{free}}$ (%)¶  | 22.2/29.8    | 21.4/30.3            | 21.0/31.2        |          |            |        |

\* $R_{\text{merge}} = \sum_h \sum_i |I_{hi} - \langle I_h \rangle| / \sum_h \sum_i I_{hi}$ , where  $h$  are unique reflection indices and  $i$  indicates symmetry equivalent indices. †Numbers in parentheses correspond to the values in the highest resolution shell. ‡ $R_{\text{der}} = \sum |F_{\text{PH}} - F_{\text{P}}| / \sum |F_{\text{P}}|$ , where  $|F_{\text{P}}|$  and  $|F_{\text{PH}}|$  refer to the measured structure factor amplitudes of the native and the derivative. §Phasing power =  $f_{\text{rms}}/E_{\text{rms}}$ , where  $f_{\text{rms}} = [(\sum f_i^2)/n]^{1/2}$  and  $E_{\text{rms}} = [(\sum (F_{\text{PH}} - |F_{\text{P}} + f_i|)^2)/n]^{1/2}$ . || $R_{\text{cullis}} = \sum (|F_{\text{P}}| - (|F_{\text{PH}}| - |F_{\text{P}}|)) / \sum (|F_{\text{PH}}| - |F_{\text{P}}|)$  (only for centric reflections), where  $|F_{\text{P}}|$  represents the calculated heavy atom structure factor. ¶ $R_{\text{work}} = \sum |F_{\text{o}} - F_{\text{c}}| / \sum F_{\text{o}}$  for all reflections and  $R_{\text{free}} = \sum |F_{\text{o}} - F_{\text{c}}| / \sum F_{\text{o}}$ , calculated on the 10% of data excluded from refinement.

in the L-valine-IleRS complex structure, an L-valine molecule is actually bound to the same site (Fig. 2C). The hydrophobic contact area of the L-valine side chain with those of Pro<sup>46</sup> and Trp<sup>558</sup> is slightly smaller than that of the L-isoleucine side chain (Fig. 2, B and C), which is consistent with the calculation by Pauling (5) and with previous kinetics (3). All of these results agree with the concept of the first, coarse sieve in the double-sieve mechanism of editing (2). All of the amino acid residues that form the amino acid-binding pocket, except Gln<sup>554</sup>, are conserved in the ValRSs (12). In contrast, ValRS has an invariant Pro as a substitute for Gly<sup>45</sup> neighboring Pro<sup>46</sup>, which may narrow the space within the hydrophobic pocket to exclude L-isoleucine. In fact, the substitution of Ala for Gly<sup>56</sup> of *Escherichia coli* IleRS, which corresponds to the Gly<sup>45</sup> of *T. thermophilus* IleRS, reduced the amino acid-binding activities and completely eliminated the discrimination between L-isoleucine and L-valine (6).

The Rossmann-fold domain has a  $\beta$ -rich insert consisting of four structural domains (Ins-1 to Ins-4) (Fig. 1). The Ins-1 and Ins-4 domains (shown in blue and light green, respectively, in Fig. 1) have zinc ions coordinated to Cys<sup>181</sup>-X<sub>2</sub>-Cys<sup>184</sup>-X<sub>204</sub>-Cys<sup>389</sup>-X<sub>2</sub>-Cys<sup>392</sup> and Cys<sup>461</sup>-X<sub>2</sub>-Cys<sup>464</sup>-X<sub>37</sub>-Cys<sup>502</sup>-X-Cys<sup>504</sup> (where X is any amino acid), respectively. The Ins-1 zinc-binding structure includes an unusually long insert between the second and third Cys residues, which encompasses the entire 191-residue globular Ins-2 domain (shown in aqua in Fig. 1). A  $\beta$ -barrel core and a protruding  $\beta$

ribbon of the Ins-2 domain form a deep cleft, the size of which is comparable to that of the catalytic cleft of the Rossmann-fold domain (Fig. 1).

The "CP1" fragment (14) (corresponding to the present Ins-1 and Ins-2 domains) cloned from *E. coli* IleRS retains the specific Val-tRNA<sup>Ile</sup> editing activity (9). In the present L-valine-IleRS complex structure, a second L-valine molecule was identified at the bottom of the deep cleft in the Ins-2 domain (Fig. 3, A and B). In contrast, in the L-isoleucine-IleRS complex structure, no electron density was observed in this second pocket (13). Therefore, the second pocket on the Ins-2 domain is specific for L-valine, indicating that this pocket is the site for the second, fine sieve of the double-sieve mechanism (2). The space made up of the invariant Trp<sup>232</sup> and Tyr<sup>386</sup> residues is just large enough to accommodate L-valine and therefore is too small for L-isoleucine (Fig. 3B). This is in striking contrast to the first pocket on the Rossmann-fold domain, where there is room for one more methyl group in the L-valine-IleRS complex structure (Fig. 2C). This result is consistent with the previous finding that the substitution of Phe for Tyr<sup>403</sup>, which corresponds to Tyr<sup>386</sup> of the *T. thermophilus* IleRS, substantially affects the editing activity of the *E. coli* IleRS (8).

To demonstrate that the cleft on the Ins-2 domain actually functions as the hydrolytic editing site, we constructed an IleRS mutant [ $\Delta(219$  to 265)] that lacks 47 amino acid residues, including the Trp<sup>232</sup> of the L-valine-specific pocket. This deletion mutation completely abolished the Val-tRNA<sup>Ile</sup> editing activity, in accordance

with our placement of the second, fine sieve at this site. This mutant exhibited nearly the same (or even slightly higher) activity for Ile-tRNA<sup>Ile</sup> synthesis [a Michaelis constant ( $K_m$ ) value of 91  $\mu$ M for L-isoleucine and a first-order rate constant ( $k_{cat}$ ) value of 0.78 s<sup>-1</sup>] as that of the wild-type IleRS (a  $K_m$  value of 45  $\mu$ M for L-isoleucine and a  $k_{cat}$  value of 0.69 s<sup>-1</sup>) (15). On the other hand, the ability of this mutant IleRS to mischarge tRNA<sup>Ile</sup> with L-valine was drastically higher (the  $K_m$  value for L-valine and the  $k_{cat}$  value are 86  $\mu$ M and 0.21 s<sup>-1</sup>, respectively) than that of the wild type (not detectable). It is surprising that the  $K_m$  value for L-valine is the same as that for L-isoleucine in the aminoacyl-tRNA formation. The discrimination factor is as small as 3.5 and agrees well with the values that had been obtained by theoretical calculations (5) and previous kinetic measurements (3). This result demonstrates that the discrimination between L-isoleucine and L-valine depends primarily on the editing reaction.

The cleft on the Ins-2 domain is now identified as the catalytic site for specific editing against Val. Manual fitting of Val-AMP and Val-tRNA<sup>Ile</sup> into this cleft confirmed that the mouth of the cleft is wide enough to accommodate the valylated products (13), but, once bound, how are the valylated products hydrolyzed? Near the L-valine-specific pocket, two absolutely conserved peptide segments come together to form the bottom of the cleft in the Ins-2 domain. The first peptide segment has a Thr-rich sequence, Trp<sup>227</sup>-Thr-Thr-Thr-Pro-Trp-Thr-X-X-X-Asn, in which the Trp<sup>232</sup> residue is involved in the L-valine-

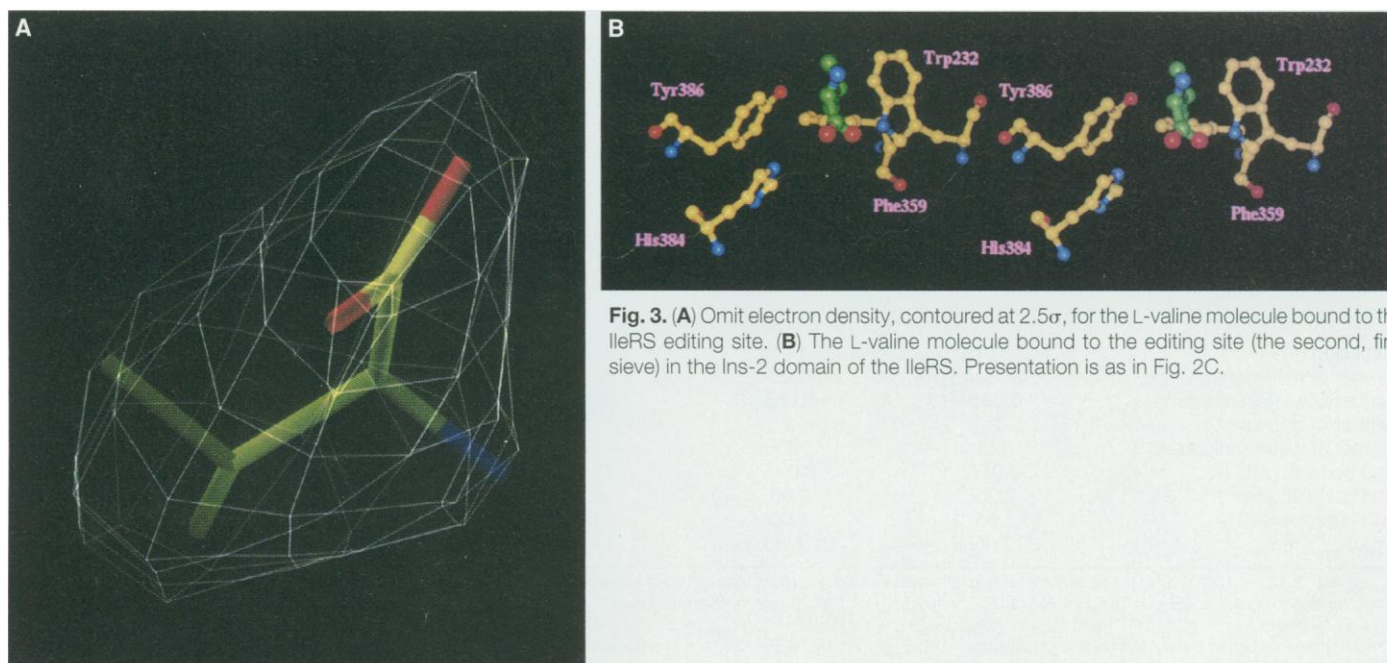


**Fig. 3.** (A) Omit electron density, contoured at  $2.5\sigma$ , for the L-valine molecule bound to the IleRS editing site. (B) The L-valine molecule bound to the editing site (the second, fine sieve) in the Ins-2 domain of the IleRS. Presentation is as in Fig. 2C.

specific pocket (Fig. 3B). The second segment has a sequence of Gly<sup>314</sup>-Thr-Gly-X-Val-His. In the present structure, Thr<sup>230</sup> in the first segment is closest to the carboxyl oxygen of the bound L-valine; the O $\gamma$  atom is 5.0 Å away from the carboxyl oxygen (Fig. 4). Furthermore, near the bound L-valine, Thr<sup>228</sup>, Thr<sup>230</sup>, Thr<sup>233</sup>, and Asn<sup>237</sup> from the first segment and His<sup>319</sup> from the second segment are located in close proximity (Fig. 4), which is reminiscent of the catalytic triads of hydrolases (16–18). Finally, a water molecule was found to be tightly bound in the editing cleft (Fig. 4).

Further mutagenesis analyses were made on the *E. coli* IleRS (19), which has been the most extensively studied IleRS in terms of editing catalysis (2–4, 6–9, 20). Ala mutations of Thr<sup>243</sup> and Asn<sup>250</sup>, which correspond to Thr<sup>230</sup> and Asn<sup>237</sup>, respectively, of *T. thermophilus* IleRS, completely abolished editing activity against Val, with little change in aminoacylation activity. In contrast, Ala mutants of Thr<sup>241</sup> and Thr<sup>246</sup>, corresponding to the *T. thermophilus* Thr<sup>228</sup> and Thr<sup>233</sup>, respectively, showed nearly the same editing activities as the wild-type enzyme (21). These mutagenesis results confirm the identity of this cleft as the editing site and the catalytic importance of both Thr<sup>230</sup> and Asn<sup>237</sup>.

ValRS also exhibits an editing activity, which deacylates Thr-AMP and Thr-tRNA<sup>Val</sup> (3, 7). A sequence alignment between IleRSs and ValRSs revealed that ValRSs also have two corresponding invariant peptide segments, Ala-Thr-X-Arg-Pro-Glu-Thr-X-X-X-Asp and Gly-Thr-Gly-X-

Lys. The invariant Asp and Lys residues of ValRSs correspond to Asn<sup>237</sup> and His<sup>319</sup>, respectively, of *T. thermophilus* IleRS. The Trp residue in the L-valine-specific pocket of the IleRS is switched to the invariant Glu residue, which may recognize the hydrophilic side chain of the misactivated L-threonine.

The present findings show that the “editing” reaction is the latter half of a stepwise substrate selection and is not an ordinary error correction. Therefore, this reaction is unique among the essential editing or proof-reading processes necessary to achieve high accuracy of information transfer in the central dogma (replication, transcription, and translation) (1, 2). The ATP consumption with regard to L-valine is nonproductive and is solely for substrate selection, which demonstrates the high cost of accuracy. The Ile-Val discrimination is biologically important. For example, a single Ile-Val mutation reduces protein stability (22) and has a substantial effect on biological phenomena, such as lung cancer susceptibility (23) and human immunodeficiency virus-1 drug resistance (24). On the other hand, it is interesting from an evolutionary viewpoint that all of the enzymes catalyzing the central steps of Ile-Val biosynthesis and metabolism do not distinguish, or can neglect the difference, between the two aliphatic amino acids, as was observed for the first catalytic site of IleRS. This finding implies that a putative ancestral enzyme of IleRS and ValRS might have actually had a similar dual specificity for L-isoleucine and L-valine in a primordial genetic code system.

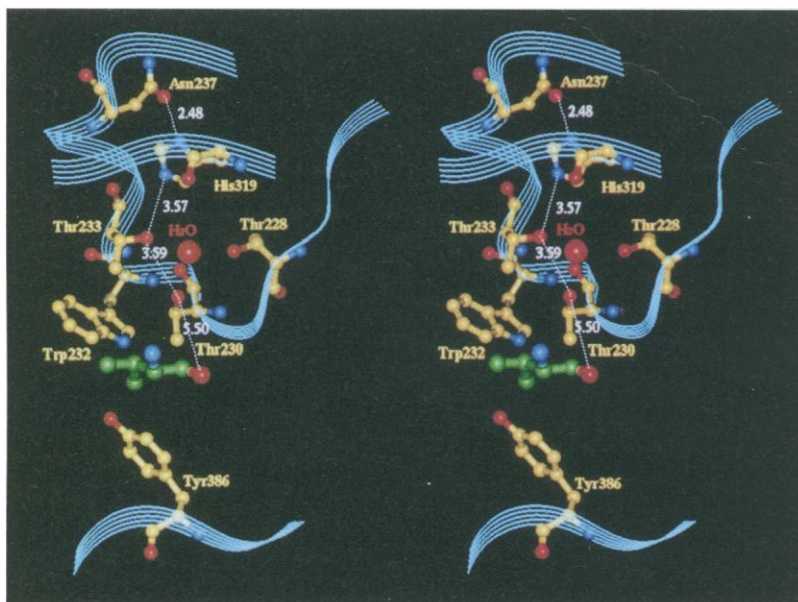


**Fig. 4.** Stereoview of the IleRS editing site as a ball-and-stick representation. The nitrogen and oxygen atoms are shown in dark blue and red, respectively. The carbon atoms of the essential residues in IleRS and those of the bound L-valine are shown in yellow and green, respectively. The tightly bound water molecules are shown as large red balls.

## REFERENCES AND NOTES

1. J. J. Hopfield, *Proc. Natl. Acad. Sci. U.S.A.* **71**, 4135 (1974); J. Ninio, *Biochimie* **57**, 587 (1975); S. M. Burgess and C. Guthrie, *Trends Biochem. Sci.* **18**, 381 (1993); A. N. Baldwin and P. Berg, *J. Biol. Chem.* **241**, 839 (1966).
2. A. Fersht, *Enzyme Structure and Mechanism* (Freeman, New York, 1985); *Biochemistry* **16**, 1025 (1977); A. R. Fersht and C. Dingwall, *ibid.* **18**, 2627 (1979).
3. W. Freist, I. Pardowitz, F. Cramer, *Biochemistry* **24**, 7014 (1985).
4. W. Freist, *ibid.* **28**, 6787 (1989).
5. L. Pauling, in *Festschrift Arthur Stroll* (Birkhäuser-Verlag, Basel, Switzerland, 1957), pp. 597–602.
6. E. Schmidt and P. Schimmel, *Science* **264**, 265 (1994).
7. E. W. Eldred and P. Schimmel, *J. Biol. Chem.* **247**, 2961 (1972).
8. E. Schmidt and P. Schimmel, *Biochemistry* **34**, 11204 (1995).
9. L. Lin, S. P. Hale, P. Schimmel, *Nature* **384**, 33 (1996).
10. The *T. thermophilus* IleRS gene was cloned into a T7 polymerase expression vector and was overexpressed in *E. coli* strain JM109(DE3) (S. Fukai *et al.*, in preparation). The recombinant protein was purified by a combination of heat treatment, anion-exchange chromatography, and reversed-phase fast performance liquid chromatography. Crystals were grown at 20°C by the hanging-drop vapor diffusion method (protein concentration of 20 mg/ml) against a reservoir solution containing 12% polyethylene glycol 4000, 6% isopropanol, 1% 2-methyl-pentane-2,4-diol, and 60 mM Hepes (pH 7.5). Two mutant proteins, with substitutions of Cys for Ala or Lys, were expressed, purified, and used for the preparation of mercury derivatives. Furthermore, we incorporated selenium into the IleRS by preparing the IleRS from the *E. coli* Met-auxotroph B834 strain cultured in the presence of selenomethionine. Crystals of the Cys- and selenomethionine-substituted proteins were grown by cross seeding. Heavy atom derivatives were prepared by cocrystallization of the Cys mutants and methylmercurichloride. Native and heavy atom derivative data were collected to 2.5 Å with a Weissenberg camera for macromolecules installed on the beam line 6A2 at the Photon Factory (Tsukuba, Japan). The data set for crystal of selenomethionine-substituted IleRS was collected in-house on a Raxis-Ilc (Rigaku, Tokyo, Japan) image plate detector mounted on a Rigaku x-ray source. All of the data were processed with the DENZO and SCALEPACK programs (25). Subsequent calculations were carried out with the CCP4 program suite (26). Initial mercury sites in the derivative of the K3C mutant were determined with the RSPS program (26) from an isomorphous difference Patterson map. The phases from the mercury derivative were used to locate the positions of other mercury and selenium atoms by difference Fourier analysis. Heavy-atom parameters were refined with the MLPHARE (26) program. The overall figure of merit from 50 to 3.0 Å resolution is 0.74. After density modification with solvent flattening and histogram matching in the program DM (26) and solvent flipping in the SOLOMON (27) program, the atomic model of residues 1 to 818 could be built with the program O (28). Crystallographic positional and slow-cooling refinement was carried out with X-PLOR (29). The Ramachandran plot analysis with the PROCHECK (30) program showed that 98.2% of the residues in the present structure are in the most favorable and the additionally allowed regions. We obtained the Ile and Val complexes by transferring the crystals to a harvest buffer containing 10 mM amino acid substrates. The data sets were collected on a Raxis-Ilc image plate detector. After rigid-body refinement in the program AMORE (26), the *R* factors were reduced.
11. G. Eriani, M. Delarue, O. Poch, J. Gangloff, D. Moras, *Nature* **347**, 203 (1990).
12. S. Fukai *et al.*, unpublished data.
13. O. Nureki *et al.*, data not shown.
14. R. M. Starzyk, T. A. Webster, P. Schimmel, *Science* **237**, 1614 (1987).

15. O. Nureki *et al.*, unpublished data.
16. N. D. Rawlings and A. J. Barrett, *Methods Enzymol.* **244**, 19 (1994).
17. N. C. Strynadka *et al.*, *Nature* **359**, 700 (1992).
18. M. Miller, M. Rao, A. Wlodawer, M. R. Gribskov, *FEBS Lett.* **328**, 275 (1993).
19. Charging assays: Mutants were examined for their ability to catalyze the formation of Ile-tRNA<sup>Ile</sup> under standard charging assay conditions. Final concentrations in each reaction mixture were 1 nM enzyme, 1.8  $\mu$ M tRNA<sup>Ile</sup>, 20 mM Hepes (pH 7.5), 100  $\mu$ M EDTA, 150 mM NH<sub>4</sub>Cl, bovine serum albumin (10  $\mu$ g/ml), 2 mM ATP, 4 mM MgCl<sub>2</sub>, and 20  $\mu$ M L-isoleucine. Editing assays: Each mutant was evaluated in an adenosine triphosphatase assay that measured tRNA-dependent editing by following the hydrolysis of ATP in the presence of L-valine and tRNA<sup>Ile</sup>. This type of assay does not distinguish between the hydrolysis of Val-AMP or the hydrolysis of Val-tRNA<sup>Ile</sup>. Final concentrations in each reaction mixture were 3  $\mu$ M enzyme, 4.6  $\mu$ M tRNA<sup>Ile</sup>, 140 mM Tris (pH 7.5), 3 mM ATP (labeled with P<sup>32</sup> at the gamma position, 12.5  $\mu$ Ci/ml), 0.5 mM CaCl<sub>2</sub>, 10 mM L-valine, 9.3 mM MgCl<sub>2</sub>, and pyrophosphatase (5  $\mu$ g/ml). Each time point was quenched in 1.25 ml of a solution of 2 mM sodium pyrophosphate, 8% activated charcoal, 1.4% perchloric acid, and 0.4% hydrochloric acid. After 10 min at room temperature, the charcoal was pelleted by centrifugation, and the phosphate content of 500  $\mu$ l of each supernatant was quantitated by scintillation.
20. S. P. Hale, D. S. Auld, E. Schmidt, P. Schimmel, *Science* **276**, 1250 (1997).
21. E. Schmidt and P. Schimmel, unpublished data.
22. S. F. Sneddon and D. J. Tobias, *Biochemistry* **31**, 2842 (1992); S. E. Jackson, M. Moracci, N. Masry, C. M. Johnson, A. R. Fersht, *ibid.* **32**, 11259 (1993); K. Takano *et al.*, *J. Mol. Biol.* **254**, 62 (1995).
23. Z. Y. Zhang, M. J. Fasco, L. Huang, F. P. Guengerich, L. S. Kaminsky, *Cancer Res.* **56**, 3926 (1996).
24. M. A. Farrash *et al.*, *J. Virol.* **68**, 233 (1994).
25. Z. Otwinowski and W. Minor, *Methods Enzymol.* **276**, 307 (1997).
26. CCP4: Collaborative Computational Project No 4, *Acta Crystallogr. D* **50**, 760 (1994).
27. J. P. Abrahams and A. G. W. Leslie, *ibid.* **52**, 30 (1996).
28. T. A. Jones, J.-Y. Zhou, S. W. Cowan, M. Kjeldgaard, *Acta. Crystallogr. A* **47**, 110 (1991).
29. A. T. Brünger, *X-PLOR: A System for X-Ray Crystallography and NMR* (Yale Univ. Press, New Haven, CT, 1992).
30. R. A. Laskowski, M. W. MacArthur, A. L. Morris, J. M. Thornton, *J. Appl. Crystallogr.* **26**, 283 (1993).
31. J. J. Perona *et al.*, *Proc. Natl. Acad. Sci. U.S.A.* **88**, 2903 (1991).
32. We thank M. Nakasako, N. Kamiya, M. Yamamoto, H. Iwasaki, T. Ueki, and Y. Maeda for data collection and helpful discussions; N. Watanabe and N. Sakabe for help with synchrotron data collection at the Tsukuba Photon Factory; and K. Nagai and A. Murzin for helpful comments. Supported in part by Grants-in-Aid for Scientific Research on Priority Areas (04272103 and 09278102) to S.Y. from the Ministry of Education, Science, Culture, and Sports of Japan and by grant GM15539 to P.S. and T.H. from NIH. T.H. is an NIH Postdoctoral Fellow. The coordinates for *T. thermophilus* IleRS have been deposited in the Brookhaven Protein Data Base (1ILE).

15 December 1997; accepted 24 March 1998

## Dependence of Germinal Center B Cells on Expression of CD21/CD35 for Survival

Michael B. Fischer,\* Siegfried Goerg,\* LiMing Shen, Andrey P. Prodeus, Christopher C. Goodnow, Garnett Kelsoe, Michael C. Carroll†

Affinity-driven selection of B lymphocytes within germinal centers is critical for the development of high-affinity memory cells and host protection. To investigate the role of the CD21/CD35 coreceptor in B cell competition for follicular retention and survival within the germinal center, either Cr2<sup>+</sup> or Cr2<sup>null</sup> lysozyme-specific transgenic B cells were adoptively transferred into normal mice immunized with duck (DEL) or turkey (TEL) lysozyme, which bind with different affinities. In mice injected with high-affinity turkey lysozyme, Cr2<sup>null</sup> B cells responded by follicular retention; however, they could not survive within germinal centers. This suggests that CD21 provides a signal independent of antigen that is required for survival of B cells in the germinal center.

The murine Cr2 locus encodes complement receptors CD21 (CR2; 150 kD) and CD35 (CR1; 190 kD) that are expressed primarily on B cells and follicular dendritic cells (FDCs) (1). Cr2<sup>null</sup> mice have impaired immune responses to T-dependent antigens (2, 3); the defect is in the B cell compartment (2, 4). The natural ligands for CD21 and CD35 are activation products of complement C3 (C3d and C3b, respectively) (5) that are covalently coupled to antigen (6); mice deficient in C3 have impaired

humoral responses similar to those observed in Cr2<sup>null</sup> animals (7). In studies in which fusion proteins of C3d and hen egg lysozyme (HEL) were used, B cell activation in vitro and in vivo was enhanced and dependent on the presence and density of C3d (8). Thus, CD21/CD35 may be a potent coreceptor for complement-decorated antigens that can raise the intensity of sub-optimal activating signals.

To examine directly the fate of B cells deficient in CD21/CD35 in an immune recipient, we bred Cr2<sup>null</sup> mice with mice expressing a transgenic (tg) immunoglobulin (Ig) consisting of both heavy and light chains, which bind avian egg lysozymes with very high affinity (9). The importance of CD21/CD35 as a coreceptor in B cell activation by antigen ligands that bind with increasingly substantial affinities was examined by comparing the response of Cr2<sup>+</sup> and Cr2<sup>null</sup> lysozyme-specific Ig tg B cells to DEL and TEL, respectively (10, 11). As

expected, 10- to 100-fold less TEL than DEL was required for the induction of proliferative responses and up-regulation of the CD86 costimulator molecule in both groups of tg B cells (12). Thus, activation through the B cell receptor (BCR) in the absence of complement is comparable in Cr2<sup>+</sup> and Cr2<sup>null</sup> tg B cells, and B cell activation and proliferation is proportional to antigen affinity.

To examine the importance of B cell expression of CD21/CD35 in combination with low-affinity antigen (DEL) in vivo, we adoptively transferred splenic B cells isolated from either Cr2<sup>+</sup> or Cr2<sup>null</sup> lysozyme-specific Ig tg mice with DEL into wild-type (WT) recipients that had been primed 7 days earlier with DEL (13, 14). Cr2<sup>null</sup> tg B cells from the spleen declined over the 5-day period in the DEL-primed recipients (Fig. 1A); by day 5 after transfer, there were 75% fewer Cr2<sup>null</sup> than Cr2<sup>+</sup> tg B cells (0.26  $\pm$  0.04% versus 1.14  $\pm$  0.26%, respectively; *P* < 0.01) in the recipient spleens (15). An increase in Cr2<sup>null</sup> tg B cells in the blood was observed by day 5 (Fig. 1B); however, this did not account for the loss of cells from the spleen given the relatively low number of B cells in blood compared with spleen. Loss of Cr2<sup>null</sup> tg cells from the spleen was confirmed by immunohistochemical analysis (Fig. 2, A to D, and Table 1) and correlated with a low frequency of expression of CD86 (B7-2) at day 1 after transfer (12). Although similar numbers of Cr2<sup>+</sup> and Cr2<sup>null</sup> tg B cells were present on day 1 in the primary splenic follicles of immune recipients (Fig. 2, A and C), by day 5 less than 2% of follicles held Cr2<sup>null</sup> tg B cells compared with 85% of follicles positive for Cr2<sup>+</sup> tg B cells (Fig. 2, B and D, and Table 1) (16). The loss of the Cr2<sup>null</sup> tg B cells in DEL-immune recipients was greater than that in nonimmune con-

M. B. Fischer, S. Goerg, L. Shen, A. P. Prodeus, M. C. Carroll, Department of Pathology, Harvard Medical School, Boston, MA 02115, USA.

C. C. Goodnow, Medical Genome Centre, John Curtin School of Medical Research, Australian National University, Canberra, ACT 2601, Australia.

G. Kelsoe, Department of Microbiology and Immunology, University of Maryland School of Medicine, Baltimore, MD 21201-1509, USA.

\*These authors contributed equally to this work.

†To whom correspondence should be addressed. E-mail: mcarroll@warren.med.harvard.edu